Nanotube Electromechanics Beyond Carbon:

The Case of WS_2

Roi Levi[‡,†]*; Jonathan Garel,*[‡,†]*; David Teich*[§]*; Gotthard Seifert*[§]*; Reshef Tenne*[‡]*;*

Ernesto Joselevich[‡,*]

[‡]Department of Materials and Interfaces, Weizmann Institute of Science, Israel

[§]Theoretische Chemie, Technische Universität Dresden, Germany

Supporting Information

WS_2 NT synthesis. The growth mechanisms of WS_2 nanotubes (NT) can be divided into two: outside-in sulfurization (OS) of long suboxide ($W_{18}O_{49}$) nanowhiskers,[1] or a vapor-solid (VS) growth of an incipient WS_2 NT, where a volatile tungsten oxide phase is continuously sulfurized at the tip of the INT by H_2S gas.[2] The WS_2 NTs used here, were synthesized using the commonly used outside-in sulfurization method, similar to that used for the INT detailed in the FET research,[3] were synthesized by Nanomaterials Inc.[4] Here WO_{3-x} nanoparticles elongate under reducing atmosphere ($1\%H_2/99\%N_2$) to tungsten suboxide nanowhiskers which are subsequently converted to WS_2 NTs by sulfurizing the needlelike WO_{3-x} precursors.[2, 5-7] The INT empty core is the result of the difference between the oxide and sulfide densities.

These mechanisms produce WS_2 NTs with distinct structural differences. The VS WS_2 NTs are perfectly cylindrical, crystalline, open ended, slender (length~2-500 μm, diameter~15−20nm) with the most distinctive feature being the thin walls (5−8 layers) and the large hollow core (up to 70 vol%). The OS WS_2 NTs exhibit diameters of 40-250 nm with numerous shells and are almost exclusively capped at one of their ends and in some cases capped on both ends.

AFM cantilever response during measurement

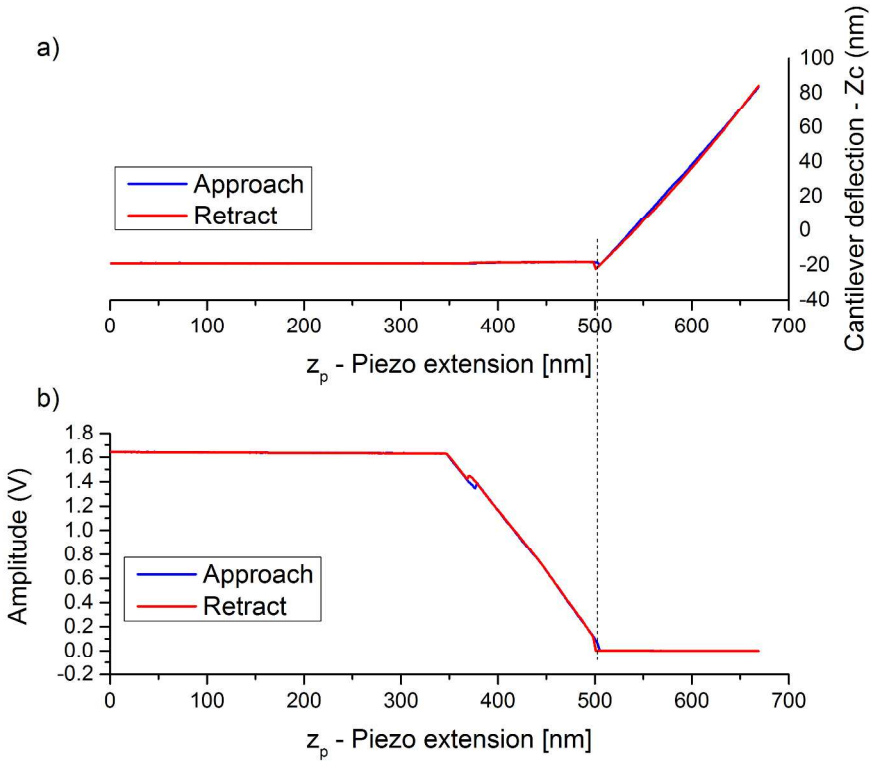

Figure S1. a) AFM tip oscillation amplitude and b) Force-distance (cantilever deflection) measurements recorded upon pressing on the pedal (right). The contact point is indicated by the tapping amplitude reaches zero (dashed line). The tapping mode deflection then increases linearly, corresponding to cantilever deformation indicated by the linear slope. The yielding of the pedal to the force results in a decreased cantilever deformation and therefore a smaller slope.

Mechanical properties. The mechanical properties of 17 WS_2 nanotubes (NT), specifically the torsional spring constant κ and the shear modulus G, were obtained from these measurements (Table S1). Here the first is the property of the torsional device, the second is an extrinsic property of the inorganic NT (INT) and the third is an intrinsic property of the INT torsional stiffness. The WS_2 NT was twisted by pressing the pedal at a series of points along the long axis of the pedal with an atomic force microscope (AFM) tip. Care was taken to maintain low torsion angles (< 20°), so as to avoid elastic to plastic transition, which may arise at high torsion angles. Additional care was taken by fabricating pedals with dimensions and materials identical to those

used in previous studies. These aforementioned pedals were studied in order to rule out possible artifacts arising from pedal deformation,[8] thus ensuring that the measured properties are those pertaining to the WS_2 NT itself.

For each point, K is calculated from eq. 1, where k_c is the spring constant of the cantilever, z_p is the Z-axis piezo extension, and z_c *is* the Z-axis cantilever deflection of the cantilever (see Fig. 1d).[9, 10]

$$K = k_c z_c / (z_p - z_c) \quad (1)$$

K is plotted against the position (x) along the pedal (see Fig. 1d), and fitted to Eq. 2, a modified leverage equation allowing for axis displacement (see Fig. 1d) where x-a is the lever arm , a is the pedal center location and K_B is the WS_2 NT bending spring constant, the latter two and the torsional spring constant κ being left as floating parameters.[10]

$$K = \left[(x-a)^2/2\kappa + {K_b}^{-1}\right]^{-1} \quad (2)$$

Using this method allows for the separation of the lever-arm dependent and independent components such as twisting as opposed to bending and slack, respectively.

The shear modulus G, is calculated using classical elasticity theory for a cylinder under torsion (eq. 7) where L is the length of the suspended segments of the WS_2 NT, and r_{in} and r_{out} are the inner and outer radii of the cylinder, respectively.[10, 11]

$$F_z = k_{\text{cantilever}} \cdot z_{\text{cantilever}} = k_{\text{INT,bend}} \cdot h_{\text{pedal,bend}} \quad (3)$$

$$\tau = F_z \cdot x = \kappa_{\text{INT}} \cdot \phi \quad (4)$$

$$z_{\text{piezo}} = z_{\text{cantilever}} + h_{\text{pedal,bend}} + h_{\text{pedal,twist}} \quad (5)$$

$$\phi = \tan^{-1}\left[\left(z_{\text{piezo}} - z_{\text{cantilever}} - h_{\text{pedal,bend}}\right)/x\right] \quad (6)$$

$$G = 2\kappa L/[\pi({r_{\text{out}}}^4 - {r_{\text{in}}}^4)] \quad (7)$$

Here the inner radii is a function of n, the number of mechanically coupled layers twisting together,[12] and thus a measure of the WS_2 NT inter-layer mechanical coupling. At the extreme values of n, the INT is treated as a solid rod (G_s) or a single layer INT (G_h). Thus for the first case Eq. 7 is reduced to Eq. 8 or to Eq. 9 for the second when using the interlayer spacing for WS_2, 6.2Å.[13]

$$G_r = 2\kappa L/(\pi {r_{out}}^4) \quad (8)$$

$$G_l = 2\kappa L/(4\pi {r_{out}}^3 \delta r) \quad (9)$$

It is possible to consider the moderate case where it is treated as a hollow-core cylinder where the inner radius is taken to be half of the outer.[3] However as the fourth power on the radii results in a change of 6% only and within experimental error this case does not give any additional information. Finally, it is possible to use the shear modulus (G_c≈80GPa) from DFTB calculations,[14] Young's modulus measurements and mechanical measurements on WS_2 NTs synthesized by other techniques such as VS WS_2 NTs.[12, 14]. In cases where G_s < 80GPa this facilitates a reverse estimation of n (Table S1).

Table S1. WS_2 NT torsional mechanical properties.[1]

Device	Outer Diameter	Length	Torsional spring constant	Effective shear modulus		Mechanically coupled layers
				Solid rod	Single Layer	
#	d	L	κ	G_s	G_h	n
	[nm]	[nm]	[N*m*10^{15}]	[GPa]		
1	30.7±3.2	330±10	10.3±0.5	39.5±11.9	243.8±55.5	3.9±2.7
2	34.8±2.2	320±10	27.7±1.4	51.5±6.6	376.9±38.9	6.7±1.6
3	37±0.9	310±10	32.9±1.5	56.7±5.2	423.3±32.3	7.9±1.4
4	39.8±0.3	320±10	42.6±1.3	55.3±2.4	443.7±18.7	8.2±0.6
5	40.2±3.2	260±10	15.4±0.4	12±0.6	103.7±4.7	1.4±0.7
6	46.7±1.7	420±10	109.8±4.2	99.6±11.2	935.7±83.3	
7	48.2±19	320±10	25.2±1.9	4.7±0.4	61.3±4.8	0.8±0.2
8	49.3±4.8	300±10	43.9±1.7	31.5±2	312.6±17.3	4.7±0.7
9	49.2±8.9	410±10	64±1.7	24.2±3.3	259.6±27.2	3.7±1.9
10	53.1±16.7	140±10	146.1±13.7	10±1.5	135.3±17.9	1.8±1.9
11	55.2±1.5	420±10	254±15	117±11.3	1302.3±108.4	
12	58.3±1.3	290±10	92±8.3	23.2±2.7	273.3±29.1	3.9±1.2
13	59.7±4	320±10	201±6.2	40.8±1.6	519.2±20.1	8.3±0.5
14	65.9±1.4	390±10	87.4±7.7	18.5±2	245.7±24.8	3.4±1.1
15	67.8±3.4	430±10	115.8±6.8	23.7±3.8	324.3±41.4	4.6±2.7
16	89±2.6	400±10	328.3±14.3	22.3±2.2	395.7±32	5.6±2.1
17	127.1±1.8	470±10	328.5±35	6±0.7	154.8±17.3	2±1.4

[1] L: suspended length. The error for d is the standard deviation of 4 measurements performed along the WS_2 NT length while the error for L is derived from the AFM topography resolution. The error for all other values is derived from the previous errors. Devices 11 and 15 are depicted in Fig 1e and 1f, respectively.

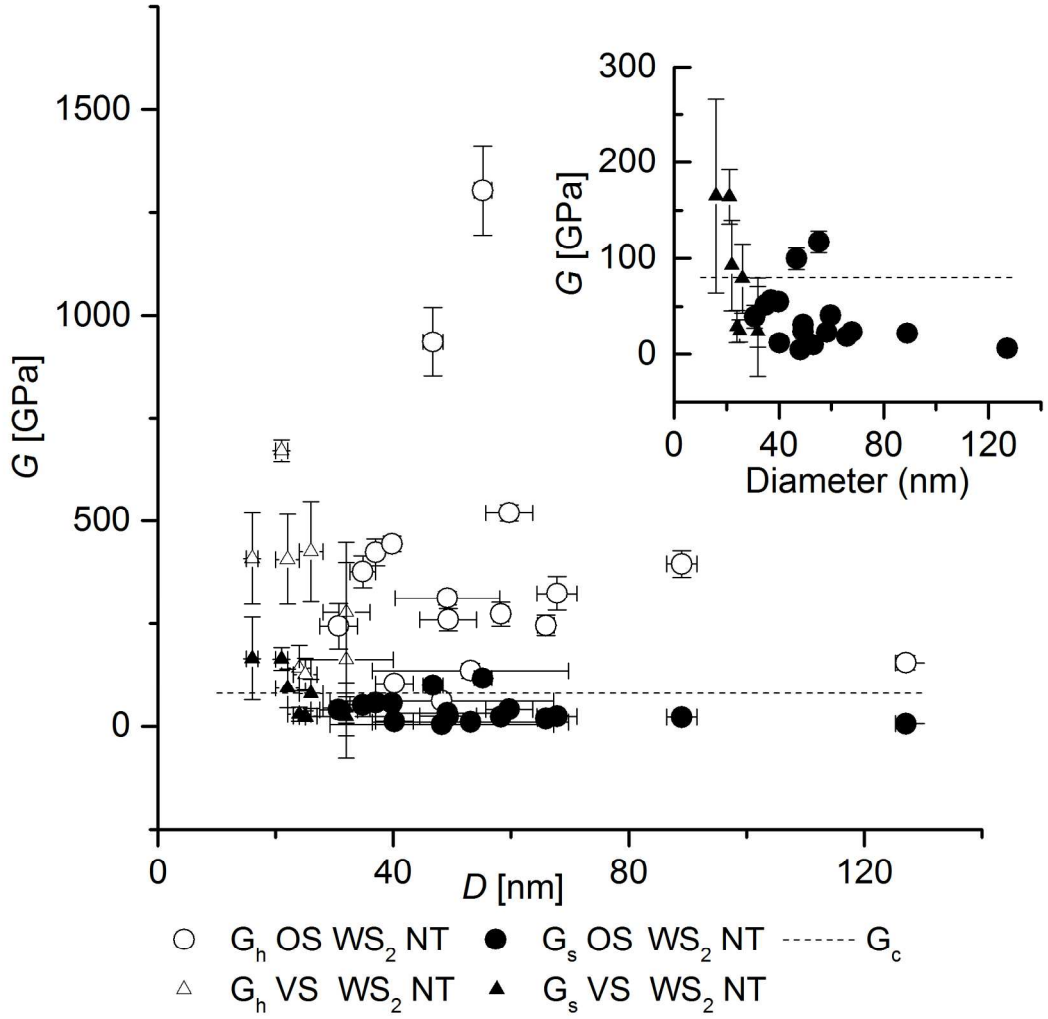

Figure S2. The effective shear modulus as a function of the nanotube diameter for OS WS_2 NTs and VS WS_2 NTs (circles and triangles, respectively) synthesized by different techniques. The effective shear moduli are calculated assuming either negligible or infinite inter-layer coupling, *i.e.* "hollow cylinder" (G_h) and "solid rod" (G_s) cases (hollow and full markers, respectively). The expected intra-layer shear modulus calculated by DFTB (G_c) is shown as a reference.[12] Inset – close-up of the solid rod case values. The horizontal and vertical error bars correspond to the standard deviation of the experimental data.

Fig. S2 plots the shear moduli data against the OS WS_2 NT diameter for the devices measured here, the VS WS_2 NTs synthesized by a different synthetic technique,[12] and the theoretical value marked by a dotted line.[14] These results show that over the entire diameter range G_h , which is calculated using a single layer case, is significantly larger than the theoretical value G_c. This indicates that a significant number of layers are twisting together. This observation is in agreement with the experimental results for VS-WS_2 NTs as well as the theoretical work on VS WS_2 NTs where it was shown that for small angles all the layers twist together. Additionally, it can be seen that for both types of WS_2 NTs, experimental G_s values larger than G_c are observed, indicating that G_{th} is possibly underestimated. Finally, the torsional spring constant κ values obtained here are up to an order of magnitude higher than BNNT,[8] and two orders of magnitude larger than CNT, indicating that WS_2 NTs possess quite a high torsional stiffness.

Comparing these results to those obtained for VS WS_2 NTs shows a similar trend,[12] albeit at higher values. Interestingly, a similar effect was observed in the telescopic shear of WS_2 NTs where nanotubes synthesized by outside-in sulfurization exhibited a larger degree of inter-layer mechanical coupling when compared to VS WS_2 NTs.[15] This is in line with the promising performance of WS_2 NTs in nanocomposites and further highlights the possible use of the WS_2 NTs in NEMS.

Electromechanical properties. After the WS_2 NTs were characterized mechanically they were connected to an AC voltage of 0.1 V with a DC bias of 5V (see section 2.3). However due to technical issues only 6 of the 17 devices were available for electromechanical measurements. Of these, 5 out of the 6 showed a consistent electromechanical response to torsion (see Fig. S3). Two devices were subjected to bending and both showed a consistent electromechanical

response. Due to the measuring equipment generating electrical noise the results presented in table S2 were obtained by averaging a large number of measurements.

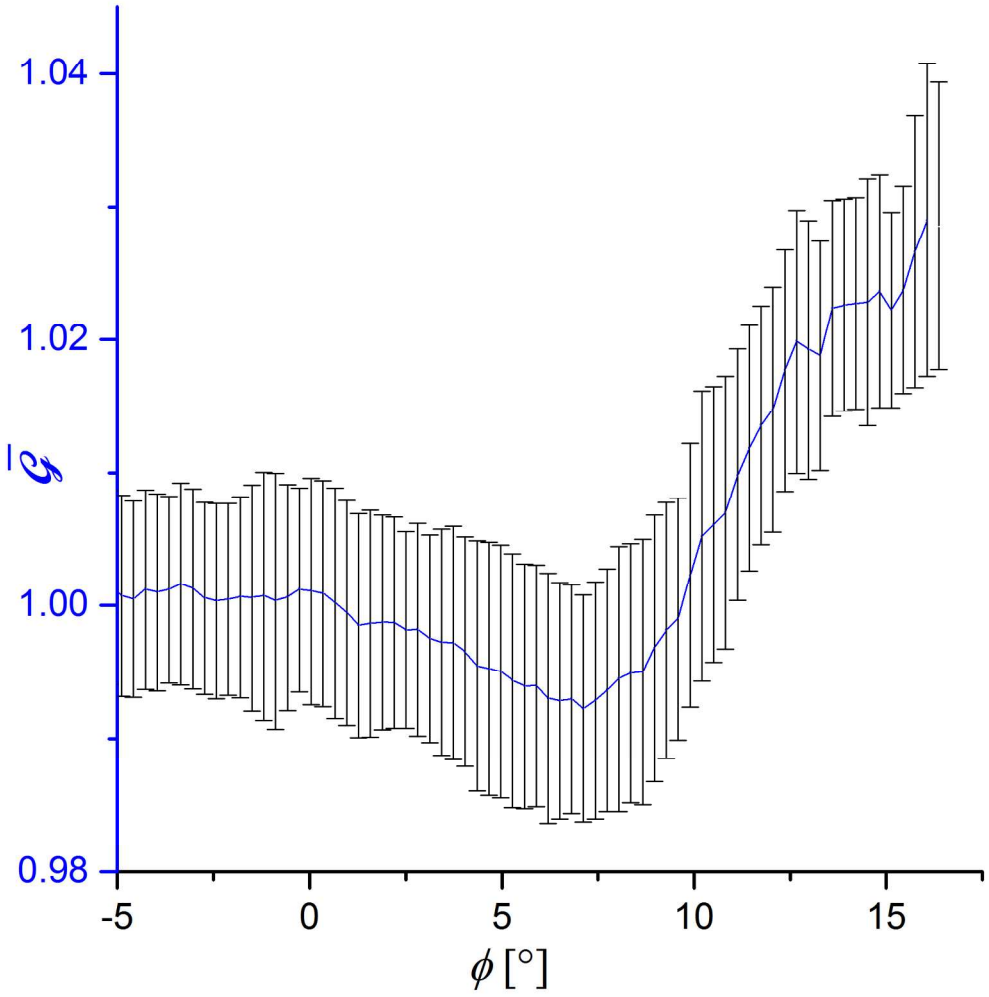

Figure S3. Repeatability of the electromechanical response with over 250 repeat twists of a WS_2 NT. The blue line shows the average value and the black lines denote the standard deviation of the average.

From this data two values are extracted – $\left(\bar{\mathcal{G}}_{\text{measured, strain}}\right)_{\text{max}}$ for bending or as $\left(\bar{\mathcal{G}}_{\text{measured, strain}}/\phi\right)_{\text{max}}$ for torsion where ϕ is the torsion angle in radians. $\left(\bar{\mathcal{G}}_{\text{measured, strain}}\right)_{\text{max}}$ is calculated for the highest overall change, while

$\left(\bar{\mathcal{G}}_{\text{measured, strain}}/\phi\right)_{\max}$ yields the maximum sensitivity of the signal at a given angle within the rise region.

Table S2. WS_2 NT mechanical and electromechanical properties under torsion and\or tension.[2]

#	d	G_s	G_h	$\left(\bar{\mathcal{G}}_{\text{measured,}/\phi}\right)_{\max}$	$\left(\bar{\mathcal{G}}_{\text{measured,}}\right)_{\max}$
	[nm]	[GPa]		[%*rad^{-1}]	[%]
1	30.7±3.2	39.5±11.9	243.8±55.5		
2	34.8±2.2	51.5±6.6	376.9±38.9		
3	37±0.9	56.7±5.2	423.3±32.3		
4	39.8±0.3	55.3±2.4	443.7±18.7		
5	40.2±3.2	12±0.6	103.7±4.7	14%	30%
6	46.7±1.7	99.6±11.2	935.7±83.3	145%	
7	48.2±19	4.7±0.4	61.3±4.8		
8	49.3±4.8	31.5±2	312.6±17.3		
9	49.2±8.9	24.2±3.3	259.6±27.2	3%	
10	53.1±16.7	10±1.5	135.3±17.9		
11	55.2±1.5	117±11.3	1302.3±108.4	0%	
12	58.3±1.3	23.2±2.7	273.3±29.1		
13	59.7±4	40.8±1.6	519.2±20.1		
14	65.9±1.4	18.5±2	245.7±24.8		
15	67.8±3.4	23.7±3.8	324.3±41.4	8%	26.0%
16	89±2.6	22.3±2.2	395.7±32	47%	
17	127.1±1.8	6±0.7	154.8±17.3		

[2] The error for d is the standard deviation of 4 measurements performed along the WS_2 NT length while the error for all other values is derived from the previous errors. Device 15 was bent by pressing on the pedal above the NT center giving a similar behavior to device 5 (the pedal curvature in this section does not allow for extraction of the lever length).

It is interesting to note that both the number of responsive devices and the electromechanical response are quite high, particularly when compared to CNT (30-350% and 23.8%, respectively).[9, 16, 17]

Density-functional-tight-binding calculations. The density-functional-tight-binding (DFTB) method is an approximate density-functional theory method.[18, 19]. The single-particle Kohn-Sham eigenfunctions are expressed as a linear combination of localized atom-centered basis function, which are determined by self-consistent density-functional calculations on isolated atoms. The effective one-electron potential in the Kohn-Sham Hamiltonian is written as a superposition of atomic potentials, and only one- and two-center integrals are calculated to set up the Hamiltonian matrix. The calculations of the twisted nanotubes utilized helical boundary conditions[20].

Calculation of the strain – band gap relationships. We start by several assumptions where n is the free charge carrier concentration based on the intrinsic semiconductor model, k_B is boltzmann's constant , T is the temperature in kelvin, ε is strain, σ is the uniaxial strain, ξ is the shear strain, Y is the measured young's modulus,[14] F_z is the vertical force and A_{cs} is the nanotube cross section calculated from d and assuming the inner radius is $d/2$:[3]

$$\mathcal{G} \propto n \tag{10}$$

More specifically that:

$$\mathcal{G} \propto n \propto exp\left(-E_g/2k_B T\right) \tag{11}$$

As was demonstrated in article we may assume a linear $\Delta E_g - \varepsilon$ relation:

$$\Delta E_g \propto \lambda\varepsilon \tag{12}$$

Thus assuming E_g alone is affected by ε as:

$$\bar{\mathcal{G}} = (\mathcal{G}_{strain}/\mathcal{G}_0) = exp\left(-E_{g,strain}/2k_B T + E_{g,0}/2k_B T\right) = exp\left(-\lambda\varepsilon/2k_B T\right) \tag{13}$$

We may then apply Eq. 13 to calculate $\bar{\mathcal{G}}_{estimated}$ for three cases where we calculate the

contribution from torsion, tension and the combination of both ($\bar{\mathcal{G}}_{\text{estimated, torsion}}$, $\bar{\mathcal{G}}_{\text{estimated, tension}}$ and $\bar{\mathcal{G}}_{\text{estimated, torsion\&tension}}$, respectively).

$$\bar{\mathcal{G}}_{\text{estimated, torsion}} = \exp\left(-\lambda_{\xi}\xi/2k_{\text{B}}T\right) \quad (14)$$

$$\bar{\mathcal{G}}_{\text{estimated, tension}} = \exp(-\lambda_{\sigma}\sigma/2k_{\text{B}}T) \quad (15)$$

$$\bar{\mathcal{G}}_{\text{estimated, torsion\&tension}} = exp\left(-\left(\lambda_{\xi}\xi + \lambda_{\sigma}\sigma\right)/2k_{\text{B}}T\right) \quad (16)$$

Where σ is calculated as:[9]

$$\sigma = 0.5(F_{\text{z}}/YA_{\text{cs}})^{2/3} \quad (17)$$

Using the torque τ and the lever length *x*-*a* extracted from the measured data.

$$F_{\text{z}} = \tau \cdot (x - a) \quad (18)$$

A qualitative comparison between $\bar{\mathcal{G}}_{\text{estimated, torsion\&tension}}$ and $\bar{\mathcal{G}}_{\text{measured}}$ is made by normalizing $\bar{\mathcal{G}}_{\text{estimated, torsion\&tension}}$ by a ratio *A* (*A*=5-10) to put them both on the same scale ($\bar{\mathcal{G}}^{*}_{\text{estimated, torsion\&tension}} = \bar{\mathcal{G}}_{\text{estimated, torsion\&tension}}/A$) as in Eq. 19-20.

$$A = \left(\Delta\bar{\mathcal{G}}_{\text{estimated, torsion\&tension}}\right)_{\text{max}}/(\Delta\bar{\mathcal{G}}_{\text{measured}})_{\text{max}} \quad (19)$$

$$\bar{\mathcal{G}}^{*}_{estimated,\ torsion\&tension} = 1 + \Delta\bar{\mathcal{G}}_{estimated,\ torsion\&tension}/A \quad (20)$$

Estimation of resistive elements in the WS_2 NTs torsional device setup. The electrical model for the device may be described as in Fig. S4:

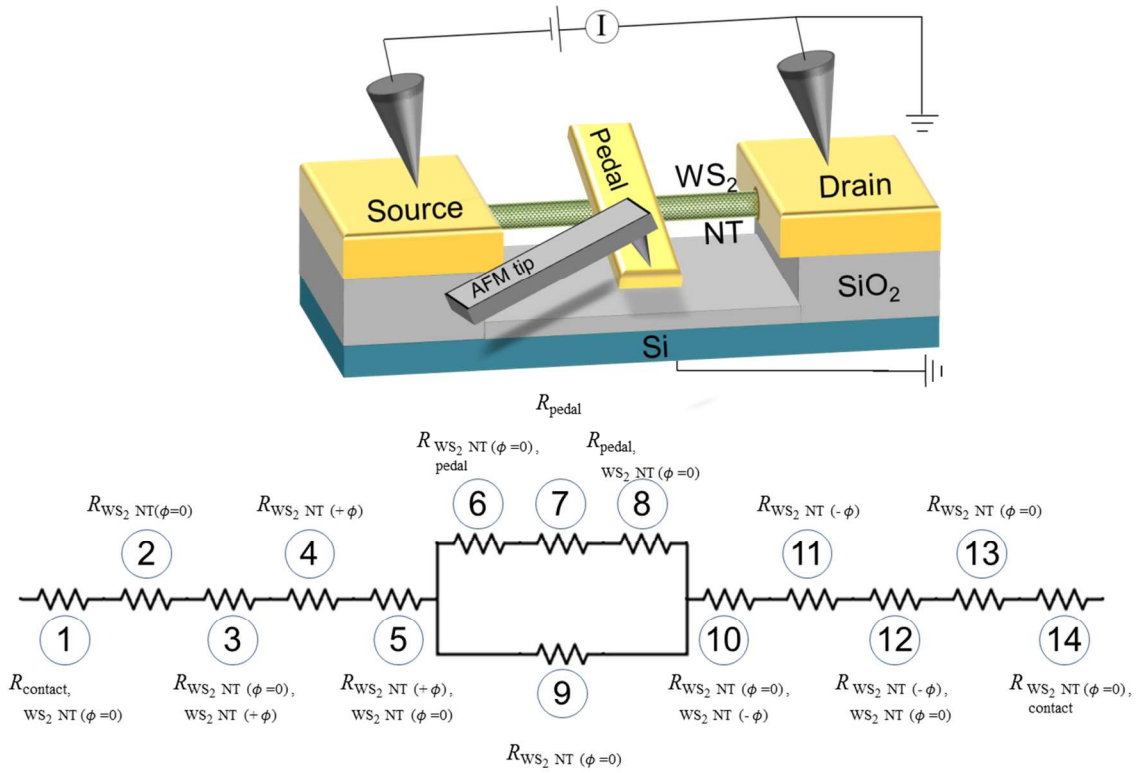

① - Contact resistance of untwisted WS_2 NT under the Cr\Au source electrode and the Cr\Au source electrode.

② - Resistance of untwisted WS_2 NT under the contact.

③ - Resistance between twisted and untwisted WS_2 NT sections.

④ - Resistance of twisted WS_2 NT section.

⑤ - Resistance between untwisted and twisted WS_2 NT sections.

⑥ - Contact resistance of untwisted WS_2 NT under the Cr\Au pedal and the Cr\Au pedal.

⑦ - Cr\Au pedal resistance.

⑧-⑭: Mirrored elements of - ⑥-①.

Figure S4. Schematic rendering of the separate resistive elements in the setup used for electromechanical measurements. a) Electromechanical measurement scheme. b) Electrical diagram of the resistive elements in the circuit.

Assuming that:

1. Twisting the INT produces a symmetric effect with respect to the twist direction. Thus the right-hand side resistors are equal to those on the left-hand side.
2. Previous 4-probe measurements are applicable here:[3]

   2.1. ⑥+⑦+⑧ >>⑨

   2.2. ① >>②+[(⑥+⑦+⑧)$^{-1}$+⑨]$^{-1}$
3. The slight differences in E_g (~10 meV) would not cause significant scattering. Thus, ③, ⑤→0.

Contact resistance and conductivity estimations. Thus, the contact resistance would remain as the dominant resistive element which is independent of ϕ. Furthermore, we then may assume that the discrepancy between the estimated and measured values is predominantly due to contact resistance (① or R_c) and calculate R_c based on this assumption.

Using Eq. 21 and 22 for the measured overall device resistance for the relaxed and twisted WS_2 NT cases (R_0 and R_ϕ, respectively) may be expressed as:

$$R_0 = 2\left(R_c + R(\phi = 0)_{WS_2\ NT}\right) \tag{21}$$

$$R_\phi = 2\left(R_c + R(\phi)_{WS_2\ NT}\right) \tag{22}$$

We may express the measured relative conductance $\bar{\mathcal{G}}_{\text{measured}}$ as:

$$\bar{\mathcal{G}}_{\text{measured}} = {R_\phi}^{-1}/{R_0}^{-1} = \left(R_c + R(\phi = 0)_{WS_2\ NT}\right)/\left(R_c + R(\phi)_{WS_2\ NT}\right) \tag{23}$$

The estimated relative conductance $\bar{\mathcal{G}}_{\text{estimated, torsion\&tension}}$ assumes $R_c = 0$ and thus:

$$\bar{\mathcal{G}}_{\text{estimated, torsion\&tension}} = R(\phi = 0)_{WS_2\ NT}/R(\phi)_{WS_2\ NT} \tag{24}$$

Finally, we may extract the contact resistance from:

$$2R_c = R_0\left({\bar{\mathcal{G}}_{\text{measured}}}^{-1} - {\bar{\mathcal{G}}_{\text{estimated, torsion\&tension}}}^{-1}\right)/\left(1 - {\bar{\mathcal{G}}_{\text{estimated, torsion\&tension}}}^{-1}\right) \tag{25}$$

Table S3. WS_2 NT measured and estimated electromechanical properties.[3]

#	Deformation	$\bar{\mathcal{G}}_{\text{estimated, torsion\&tension}}$	R_0 [MΩ]	$\bar{\mathcal{G}}_{\text{measured}}$	R_c [MΩ]	$R_c/R_{WS_2\ NT}$
5	Twisting	1.65	800	1.08	320	7
	Bending	3.00		1.30	260	6
6	Twisting	3.00	150	1.25	53	7
9	Twisting	1.40	0.18	1.01	0.088	65
15	Twisting	1.60	417	1.05	180	11
	Bending	--		1.26	--	--
16	Twisting	3.00	1.5	1.03	0.72	64

[3] Device 15 was bent by pressing on the pedal above the NT center giving a similar behavior to device 5 (the pedal curvature in this section does not allow for extraction of the lever length).

Electromechanical response extrapolation

The extrapolated electromechanical response presented here is divided into the extrapolated electrical response to torsion and the extrapolated electrical response to tension. The extrapolation of the electrical response to tension is done by taking values of σ applied to VS WS_2 NTs without any damage.[12] The extrapolation of the electrical response to tension is done by taking values of ϕ applied to OS WS_2 NTs in this work without any damage and extrapolating them to WS_2 NTs of larger diameters used in the FET research.[3] It should be noted that $\bar{\mathcal{G}}_{\text{estimated, torsion}}$ and $\bar{\mathcal{G}}_{\text{estimated, tension}}$ are not directly comparable in terms of strain values. For the sake of completion, $\bar{\mathcal{G}}_{\text{estimated, torsion}}$ as a function of the uniaxial strain (see Eq. 33 and the inset in Fig. S6a) shows a similar response to that of $\bar{\mathcal{G}}_{\text{estimated, tension}}$.

$$\sigma = \sqrt{(\xi \cdot L)^2 + L^2}/L \tag{26}$$

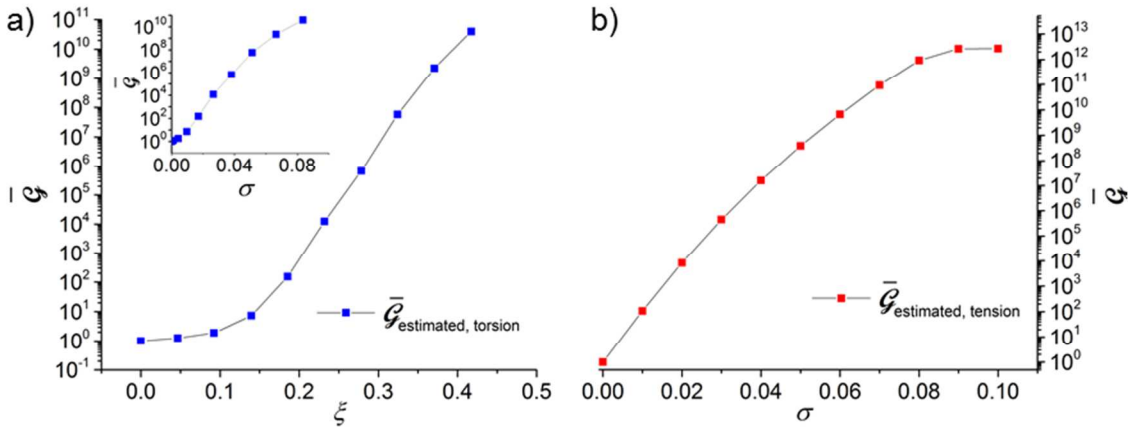

Figure S5. Extrapolation of the electrical response assuming no contact resistance to a) torsion and b) tension. The inset of a) shows $\bar{\mathcal{G}}_{\text{estimated, torsion}}$ as a function of the shear strain converted to uniaxial strain using Eq. 26 for the sake of comparison with b).

References

1. Zak, A.; Sallacan-Ecker, L.; Margolin, A.; Feldman, Y.; Popovitz-Biro, R.; Albu-Yaron, A.; Genut, M.; Tenne, R. Scaling Up of the WS_2 Nanotubes Synthesis. *Fuller. Nanotub. Car. N.* **2011**, 19, *18-26*.
2. Margolin, A.; Rosentsveig, R.; Albu-Yaron, A.; Popovitz-Biro, R.; Tenne, R. Study of the Growth Mechanism of WS_2 Nanotubes Produced by a Fluidized Bed Reactor. *J. Mater. Chem.* **2004**, 14, *617-624*.
3. Levi, R.; Bitton, O.; Leitus, G.; Tenne, R.; Joselevich, E. Field-Effect Transistors Based on WS_2 Nanotubes with High Current-Carrying Capacity. *Nano Lett.* **2013**, 13, *3736-3741*.
4. Zak, A.; Sallacan-Ecker, L.; Margolin, A.; Genut, M.; Tenne, R. Insight Into the Growth Mechanism of WS_2 Nanotubes in the Scaled-Up Fluidized-Bed Reactor. *Nano* **2009**, 4, *91-98*.
5. Rothschild, A.; Frey, G. L.; Homyonfer, M.; Tenne, R.; Rappaport, M. Synthesis of bulk WS_2 nanotube phases. *Mater. Res. Innov.* **1999**, 3, *145-149*.
6. Rothschild, A.; Sloan, J.; Tenne, R. Growth of WS_2 Nanotubes Phases. *J. Am. Chem. Soc.* **2000**, 122, *5169-5179*.
7. Rothschild, A.; Popovitz-Biro, R.; Lourie, O.; Tenne, R. Morphology of Multiwall WS_2 Nanotubes. *J. Phys. Chem B* **2000**, 104, *8976-8981*.
8. Garel, J.; Leven, I.; Zhi, C.; Nagapriya, K. S.; Popovitz-Biro, R.; Golberg, D.; Bando, Y.; Hod, O.; Joselevich, E. Ultrahigh Torsional Stiffness and Strength of Boron Nitride Nanotubes. *Nano Lett.* **2012**, 12, *6347-6352*.

9. Cohen-Karni, T.; Segev, L.; Srur-Lavi, O.; Cohen, S. R.; Joselevich, E. Torsional Electromechanical Quantum Oscillations in Carbon Nanotubes. *Nat. Nanotechnol.* **2006**, 1, *36-41*.
10. Jiang, H.; Yu, M. F.; Liu, B.; Huang, Y. Intrinsic Energy Loss Mechanisms in a Cantilevered Carbon Nanotube Beam Oscillator. *Phys. Rev. Lett.* **2004**, 93, *185501*.
11. Celik-Aktas, A.; Zuo, J. M.; Stubbins, J. F.; Tang, C.; Bando, Y. Structure and Chirality Distribution of Multiwalled Boron Nitride Nanotubes. *Appl. Phys. Lett.* **2005**, 86, *133110*.
12. Nagapriya, K. S.; Goldbart, O.; Kaplan-Ashiri, I.; Seifert, G.; Tenne, R.; Joselevich, E. Torsional Stick-Slip Behavior in WS_2 Nanotubes. *Phys. Rev. Lett.* **2008**, 101, *195501*.
13. Friend, R. H.; Yoffe, A. D. Electronic Properties of Intercalation Complexes of the Transition Metal Dichalcogenides. *Adv. Phys.* **1987**, 36, *1 - 94*.
14. Kaplan-Ashiri, I.; Cohen, S. R.; Gartsman, K.; Ivanovskaya, V.; Heine, T.; Seifert, G.; Wiesel, I.; Wagner, H. D.; Tenne, R. On the Mechanical Behavior of WS_2 Nanotubes Under Axial Tension and Compression. *Proc. Natl. Acad. Sci. U.S.A* **2006**, 103, *523-528*.
15. Tang, D.-M.; Wei, X.; Wang, M.-S.; Kawamoto, N.; Bando, Y.; Zhi, C.; Mitome, M.; Zak, A.; Tenne, R.; Golberg, D. Revealing the Anomalous Tensile Properties of WS_2 Nanotubes by in Situ Transmission Electron Microscopy. *Nano Lett.* **2013**, 13, *1034-1040*.
16. Hall, A. R.; Falvo, M. R.; Superfine, R.; Washburn, S. Electromechanical Response of Single-Walled Carbon Nanotubes to Torsional Strain in a Self-Contained Device. *Nat. Nanotechnol.* **2007**, 2, *413-416*.
17. Sazonova, V.; Yaish, Y.; Ustunel, H.; Roundy, D.; Arias, T. A.; McEuen, P. L. A Tunable Carbon Nanotube Electromechanical Oscillator. *Nature* **2004**, 431, *284-287*.

18. Seifert, G.; Porezag, D.; Frauenheim, T. Calculations of Molecules, Clusters, and Solids with a Simplified LCAO-DFT-LDA Scheme. *Int. J. Quant. Chem.* **1996**, 58, *185-192*.
19. Seifert, G. Tight-Binding Density Functional Theory: An Approximate Kohn−Sham DFT Scheme†. *J. Phys. Chem A* **2007**, 111, *5609-5613*.
20. Zhang, D.-B.; Hua, M.; Dumitrică, T. Stability of Polycrystalline and Wurtzite Si Nanowires via Symmetry-Adapted Tight-Binding Objective Molecular Dynamics. *J. Chem. Phys* **2008**, 128, *084104*.